Title No. 118-S10

# Strength and Deformation of Reinforced Concrete Squat Walls with High-Strength Materials

by Min-Yuan Cheng, Leonardus S. B. Wibowo, Marnie B. Giduquio, and Rémy D. Lequesne

*The behavior of reinforced concrete (RC) squat walls constructed with conventional- and high-strength materials was evaluated through tests of 10 wall specimens subjected to reversed cyclic loading. Primary variables included specimen height-to-length aspect ratio, steel grade, concrete compressive strength, and normalized shear stress demand. Specimens were generally in compliance with ACI 318-14. Test results showed that specimens containing conventional- and high-strength steel had similar strength and deformation capacities when designed to have equivalent steel force, defined as total steel area times steel yield stress. The lateral strength of walls with aspect ratios of 1.0 and 1.5 can be estimated using their nominal flexural strength when the nominal shear strength exceeds* $V_{mn}$*. For specimens with an aspect ratio of 0.5, the lateral strength was close to the force required to cause flexural reinforcement yielding and less than the nominal shear strength calculated per ACI 318-14. Specimen deformation capacity decreased as the normalized shear stress increased. The use of high-strength concrete, which led to a reduced normalized shear stress demand, resulted in larger specimen deformation capacity.*

**Keywords:** deformation; drift; high strength; low-rise wall; shear; squat wall; strength.

## INTRODUCTION

Reinforced concrete (RC) squat walls typically refer to walls having an aspect ratio, $h_w/l_w$, of 2.0 or less, where $h_w$ and $l_w$ are the height and length of the wall, respectively. In high-seismic regions, ACI 318-14[1] requires special boundary elements, consisting of concentrated longitudinal reinforcement and tightly spaced transverse reinforcement on the edges of squat walls, where maximum extreme fiber compressive stress corresponding to load combinations including earthquake effect exceeds 20% of the specified concrete compressive strength. This stress limit approach is very conservative, which makes the need for special boundary elements common in RC squat walls. For walls with rectangular cross sections, special boundary elements at the wall ends often result in considerable steel congestion. Using high-strength steel appears to be an attractive alternative that can reduce steel congestion.

Test results of squat walls reinforced with high-strength materials are relatively limited. Park et al.[2] tested eight squat wall specimens with $h_w/l_w$ of 1.0 to investigate the use of Grade 80 (550 MPa) high-strength steel as horizontal web reinforcement. Specimens were designed intentionally to fail in web shear prior to flexure yielding. The quantity of longitudinal reinforcement, thus, was much greater than that commonly used in practice. The shear stress imposed in most of tested specimens exceeded $10\sqrt{f_c'}$ (psi) or $0.83\sqrt{f_c'}$ (MPa), the upper limit permitted in ACI 318-14. Test results showed that the damage and failure mode of specimens reinforced with Grade 60 and Grade 80 steels were similar if the horizontal web reinforcement had equivalent steel force, defined as total steel area times steel yield stress. Test results from Cheng et al.[3] showed that squat wall specimens reinforced with high-strength steel with a specified yield stress, $f_y$, above 100 ksi (690 MPa) exhibited strength and deformation capacities like that of specimens with conventional Grade 60 steel when designed for similar shear stress demands. In that study, however, all test specimens had $h_w/l_w$ of 1.0 and concrete cylinder strength, $f_c'$, of approximately 6 ksi (41 MPa). More recently, Baek et al.[4] tested 12 wall specimens with $h_w/l_w$ of 0.5 and 1.0. Test results indicated that specimens with Grade 80 steel exhibited behavior and failure modes like those with Grade 60 steel, provided that the specimens were designed with equivalent steel force. Based on those studies, the use of high-strength steel in RC squat walls appears feasible.

This study aims to further evaluate the behavior of low-rise walls reinforced with high-strength steel by broadening the range of wall aspect ratios, $h_w/l_w$, and combining high-strength steel (yield stress greater than 100 ksi or 690 MPa) with high-strength concrete (compressive strength greater than 10 ksi or 69 MPa). A total of 10 specimens were tested under lateral displacement reversals. Variables included 1) $h_w/l_w$, 2) steel grade, 3) concrete compressive strength, and 4) normalized shear stress demand.

## RESEARCH SIGNIFICANCE

Ten large-scale wall specimens were tested to investigate the potential of using high-strength materials in RC squat walls subjected to reversed cyclic displacements. The results demonstrate the feasibility of using high-strength materials under a wider range of design variables than previously considered. Results also form the basis of recommendations for estimating the strength, deformation capacity, and stiffness of RC squat walls.

## LABORATORY TEST PROGRAM

Ten RC squat wall specimens were tested under lateral displacement reversals. These specimens were designed

*ACI Structural Journal*, V. 118, No. 1, January 2021.
MS 2020-016.R1, doi: 10.14359/51728082, received January 17, 2020, and reviewed under Institute publication policies.  Pertinent discussion including author's closure, if any, will be published ten months from this journal's date if the discussion is received within four months of the paper's print publication.

Table 1—Design parameters for test specimens

| Specimens | $h_w/l_w$ | Specified material properties | | | | $V_{n1}/V_{mpr}$ | $V_{n2}/V_{mpr}$ |
|---|---|---|---|---|---|---|---|
| | | Vertical reinforcement in SBE* $f_y$, ksi (MPa) | Web and dowel reinforcement $f_y$, ksi (MPa) | Confinement $f_y$, ksi (MPa) | $V_{mpr}/A_{cv}\sqrt{f_c'}$, psi (MPa) | | |
| (1) | (2) | (3) | (4) | (5) | (6) | (8) | (9) |
| CCC_0.5H | 0.5 | 60 (414) | 60 (414) | 60 (414) | 6 (41) | 1.07† | 1.06† |
| CHC_0.5H | 0.5 | 60 (414) | 60 (414) | 115 (785) | 6 (41) | 1.07† | 1.06† |
| HHC_0.5H | 0.5 | 115 (785) | 115 (785) | 115 (785) | 6 (41) | 1.03† | 1.09† |
| HHH_0.5H | 0.5 | 115 (785) | 115 (785) | 115 (785) | 10 (69) | 1.08† | 1.04† |
| HHH_1.0H | 1.0 | 115 (785) | 115 (785) | 115 (785) | 10 (69) | 1.07 | 1.09 |
| CCC_1.5H | 1.5 | 60 (414) | 60 (414) | 60 (414) | 6 (41) | 0.96 | 1.04 |
| HCC_1.5H | 1.5 | 100 (690) | 115 (785) | 60 (414) | 6 (41) | 0.95 | 1.06 |
| HHH_1.5H | 1.5 | 100 (690) | 115 (785) | 115 (785) | 10 (69) | 1.00 | 1.02 |
| CCC_1.5M | 1.5 | 60 (414) | 60 (414) | 60 (414) | 6 (41) | 0.97 | 1.63 |
| HCC_1.5M | 1.5 | 115 (785) | 115 (785) | 60 (414) | 6 (41) | 1.02 | 1.72 |

*SBE is special boundary element.

†$V_{mpr}$ was the shear associated with probable flexural strength at wall base without dowel reinforcement.

to complement four specimens reported by Cheng et al.,[3] which are included in the analyses later in the article. Table 1 is a test matrix with key test parameters for each specimen. Specimens were labeled as follows: the first three letters refer to the strength of the longitudinal/web steel reinforcement, confinement steel, and concrete, respectively, where $C$ stands for conventional strength and $H$ refers to high strength. The numerical value following these three letters is $h_w/l_w$. Finally, the last letter indicates the designed shear stress demand, defined as the shear stress associated with the development of the probable flexural strength, $M_{pr}$, at the wall base. A designed shear stress demand of approximately $5\sqrt{f_c'}$ (psi) or $0.42\sqrt{f_c'}$ (MPa) was considered to be moderate (M), while a designed shear stress demand exceeding $7\sqrt{f_c'}$ (psi) or $0.58\sqrt{f_c'}$ (MPa) was considered to be high (H).

The normalized shear stress demand was calculated as $V_{mpr}/A_{cv}\sqrt{f_c'}$, where $V_{mpr}$ was the probable flexural strength, $M_{pr}$, at the wall base without dowel reinforcement, divided by the distance, $h_w$, from the top of the base block to the centerline of the actuators, and $A_{cv}$ was the wall cross-sectional area determined as the wall width, $b_w$, times the wall length, $l_w$. The probable flexural strength, $M_{pr}$, was determined using the ACI 318-14 equivalent rectangular concrete stress distribution and steel stresses of $1.25f_y$ and $1.20f_y$ for specimens with Grade 60 and high-strength (USD685 or USD785) steels, respectively. Requirements of the tensile properties for USD685 and USD785 steels are summarized in Table 2. The use of $1.20f_y$ for the probable flexural strength of members using high-strength flexural reinforcement was recommended by Wibowo et al.[7]

## Test specimens

All test specimens had a nominally identical cross section of 8 x 80 in. (200 x 2000 mm). Reinforcement layouts of the wall sections are presented in Fig. 1. Each specimen consisted of a top concrete block, a wall segment, and a concrete base block (Fig. 2). The top concrete block was designed for lateral displacement/load application, and the concrete base block, anchored to the strong floor, was designed to provide fixed boundary condition at the base of the wall. Specimens were constructed in a vertical position. The concrete base block was cast first. The wall segment and top concrete block were cast together a few days later. The specified concrete compressive strength was either 6 ksi (41 MPa) or 10 ksi (69 MPa). The specified maximum coarse aggregate sizes were 3/4 in. (19 mm) and 1/2 in. (13 mm) for concrete materials with specified strengths of 6 ksi (41 MPa) and 10 ksi (69 MPa), respectively. Three types of steel reinforcement were used, Grade 60 ($f_y$ = 60 ksi [414 MPa]), USD685 ($f_y$ = 100 ksi [689 MPa]), and USD785 ($f_y$ = 115 ksi [793 MPa]). The types of steel and concrete compressive strengths specified for each wall specimen are listed in Table

Table 2—Required material properties of reinforcement

| Grade | Type | Bar size | $V_{mpr}A_{cv}f_c'$ (psi), Min. $\varepsilon_{sh}$, % | Min. $\varepsilon_u$, % | Min. $f_y$, ksi | Min. $f_p/f_y$ |
|---|---|---|---|---|---|---|
| (1) | (2) | (3) | (4) | (5) | (6) | (7) |
| Grade 60 | ASTM A706* | No. 3 to No. 6 | NA | 14 | 60 | 1.25 |
| | | No. 7 to No. 11 | | 12 | | |
| Grade 100 | USD685[6]† | — | 1.4 | 10 | 100 | 1.25 |
| Grade 115 | USD785[6]† | — | NA | 8 | 115 | NA |

*ASTM A706/A706M.[5]

†Labeled as USD685B in Aoyama.[6]

Note: 1 ksi = 6.89 MPa.

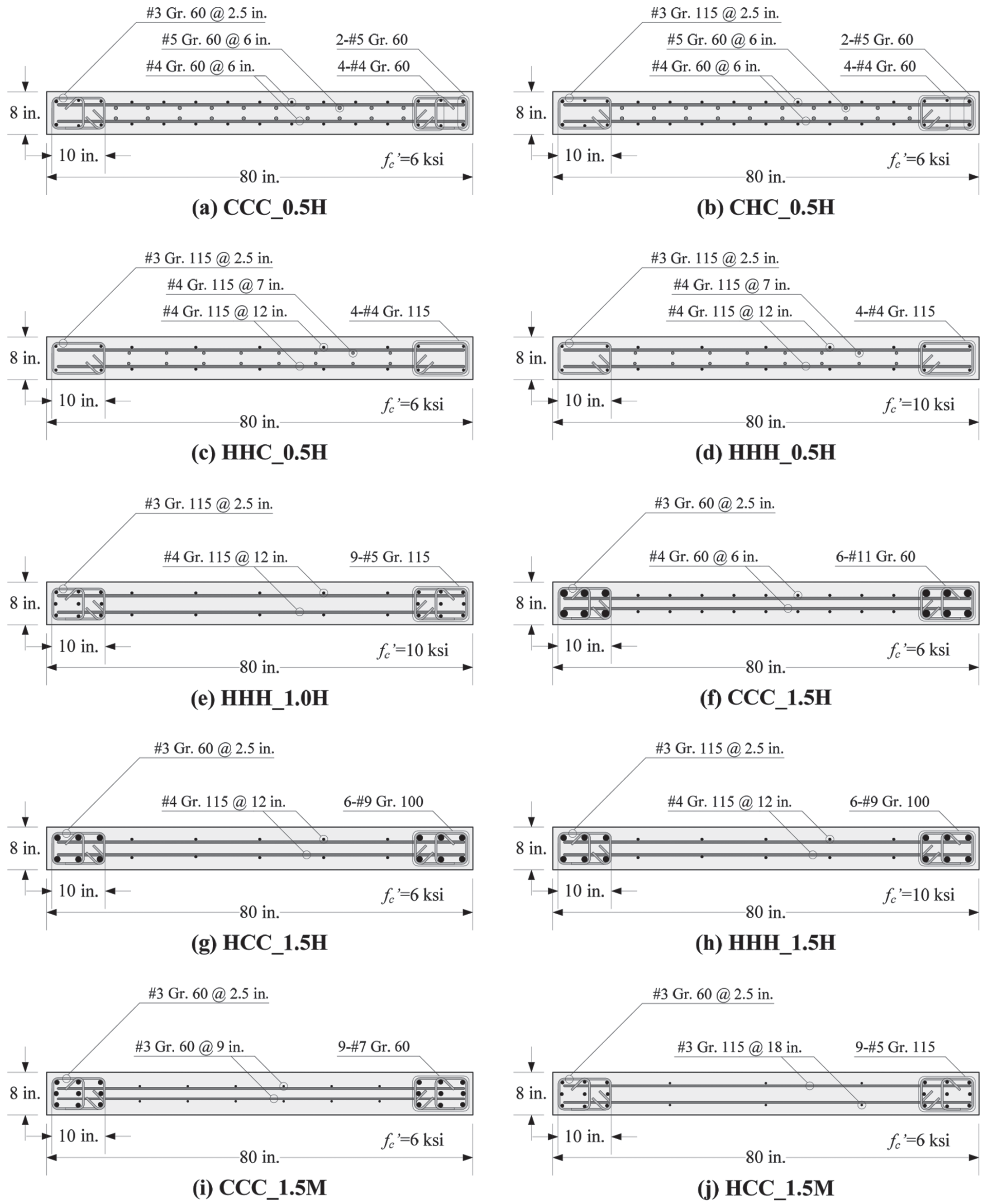


*Fig. 1—Reinforcement layout (cross section).*

1. Tested yield strengths of the various reinforcing steels used, and the cylinder compressive strengths of the concrete base block and wall section at the test date of each specimen, are listed in Table 3. Sample stress–strain results from tests of conventional- and high-strength reinforcing bars used in this study are presented in Fig. 3, where an 8 in. (200 mm) gauge length was used for strain measurement.

For CCC_0.5H, CHC_0.5H, and CCC_1.5H, longitudinal reinforcement was designed to achieve a shear stress demand of $9\sqrt{f_c'}$ (psi) or $0.75\sqrt{f_c'}$ (MPa) using Grade 60 longitudinal reinforcement and 6 ksi (41 MPa) concrete compressive strength. Specimens HHC_0.5H, and HCC_1.5H were designed to have the same shear stress demand but had high-strength longitudinal reinforcement and concrete with a compressive strength of 6 ksi (41 MPa). Longitudinal reinforcement configurations in HHH_0.5H, HHH_1.0H, and HHH_1.5H were essentially like those in HCC_0.5H, H115,[3] and HCC_1.5H, respectively, but with a concrete compressive strength of 10 ksi (69 MPa). The increase in concrete compressive strength to 10 ksi (69 MPa) in these three specimens led to a decrease in their respective shear stress demands to approximately $7\sqrt{f_c'}$ (psi) or $0.58\sqrt{f_c'}$ (MPa). For CCC_1.5M and HCC_1.5M, longitudinal reinforcement was designed to achieve a shear stress demand of $5\sqrt{f_c'}$ (psi) or $0.42\sqrt{f_c'}$ (MPa) with an $f_c'$ of 6 ksi (41 MPa). The designed shear stress demands of all test specimens are summarized in column 7 of Table 1. It should be noted, however, that specimens with $h_w/l_w$ of 0.5 were all designed with high shear stress demand to achieve a reasonable amount and spacing of vertical reinforcement.

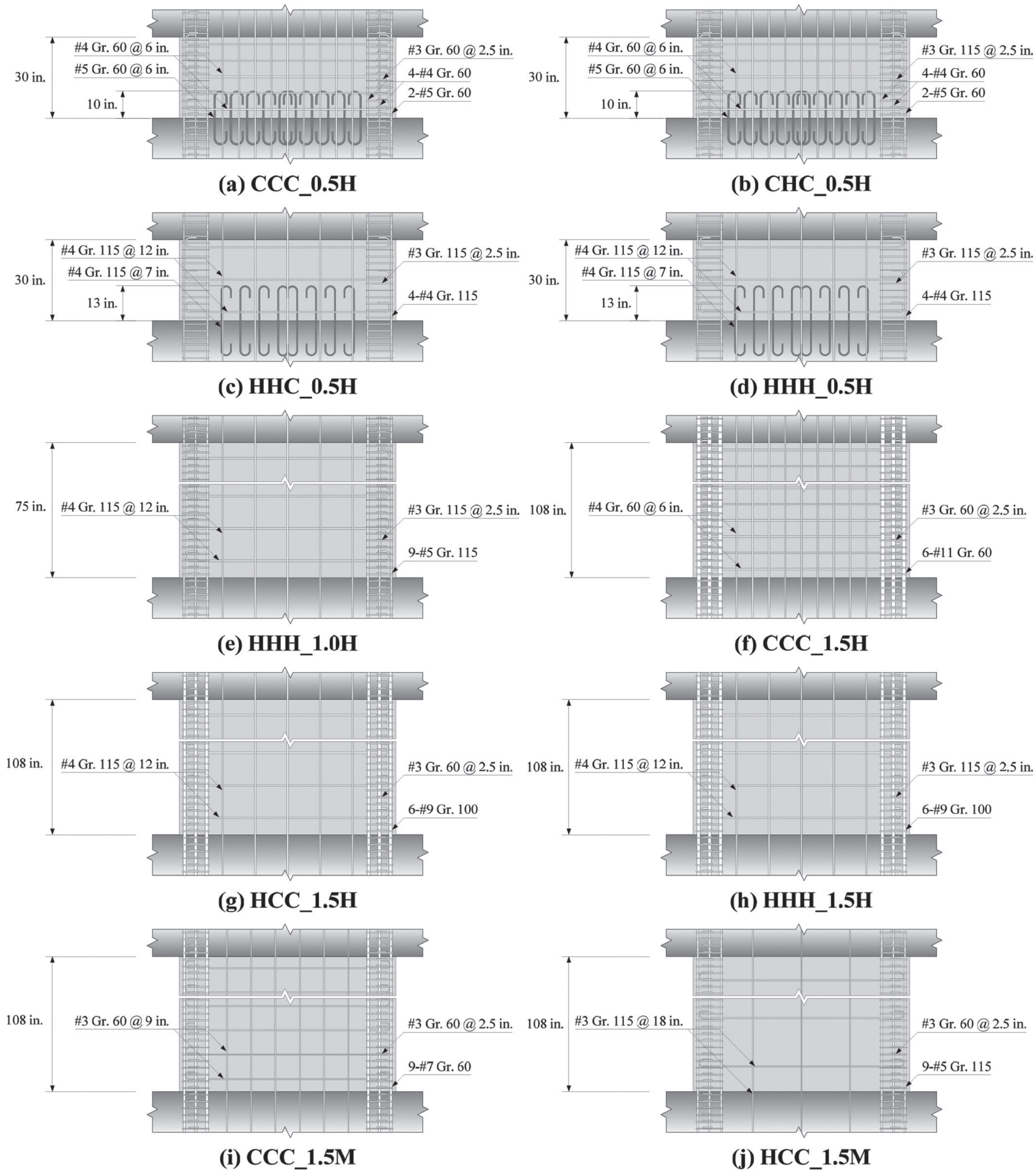


*Fig. 2—Reinforcement layout (elevation).*

Horizontal web reinforcement was provided such that the nominal shear strength calculated per ACI 318-14, as expressed in Eq. (1), was approximately equal to the design shear, that is, $V_{n1} \cong V_{mpr}$, as shown in column 8 of Table 1, where $\rho_t$ the horizontal web reinforcement ratio.

The distributed vertical web reinforcement was designed to have the same reinforcement ratio as the horizontal web reinforcement, in compliance with ACI 318-14. In addition, the total vertical reinforcement crossing the interface between the wall segment and concrete base block, $A_{vf}$, was either confirmed (for specimens with $h_w/l_w$ of 1.0 and 1.5) or designed (for specimens with $h_w/l_w$ of 0.5) to ensure that the shear frictional resistance at the wall base, $V_{n2}$, determined per Eq. (2), was greater than the design shear, that is, $V_{n2} \geq V_{mpr}$ as presented in column 9 of Table 1. The lengths of the dowel reinforcement for specimens with Grade 60 and USD785 were 10 in. (250 mm) and 13 in. (330 mm), respectively. These lengths were close to ACI 318-14 requirements for hooked-bar development.

All specimens had No. 3 (10 mm) confinement reinforcement spaced at 2.5 in. (65 mm) in the special boundary elements. Both web and confinement reinforcement satisfied the minimum amount and maximum spacing requirements of ACI 318-14. The design of CCC_1.5H violated the ACI 318-14 requirement that hoops confining No. 11 (36 mm) bars should be at least No. 4 (13 mm) bars. This specification

**Table 3—Material properties**

| | Steel reinforcement | | | | | | | | | | | | | | | | Concrete strength | |
|---|---|---|---|---|---|---|---|---|---|---|---|---|---|---|---|---|---|---|
| | SBE vertical reinforcement | | | | Web reinforcement | | | | Dowel reinforcement | | | | Confinement reinforcement | | | | Base block | Wall specimen |
| Specimen name | Bar no. | $f_y$, ksi (MPa) | $f_p$, ksi (MPa) | $f_p/f_y$ | Bar no. | $f_y$, ksi (MPa) | $f_p$, ksi (MPa) | $f_p/f_y$ | Bar no. | $f_y$, ksi (MPa) | $f_p$, ksi (MPa) | $f_p/f_y$ | Bar no. | $f_y$, ksi (MPa) | $f_p$, ksi (MPa) | $f_p/f_y$ | $f_{cm}$, ksi (MPa) | $f_{cm}$, ksi (MPa) |
| (1) | (2) | (3) | (4) | (5) | (6) | (7) | (8) | (9) | (10) | (11) | (12) | (13) | (14) | (15) | (16) | (17) | (18) | (19) |
| CCC_0.5H | No. 5 | 67.5 (465) | 102.4 (706) | 1.52 | No. 4 | 66.3 (457) | 96.1 (663) | 1.45 | No. 5 | 67.5 (465) | 102.4 (706) | 1.52 | No. 3 | 64.9 (447) | 93.9 (647) | 1.45 | 6.90 (47.6) | 5.33 (36.7) |
| | No. 4 | 66.3 (457) | 96.1 (663) | 1.45 | | | | | | | | | | | | | | |
| CHC_0.5H | No. 5 | 67.5 (465) | 102.4 (706) | 1.52 | No. 4 | 66.3 (457) | 96.1 (663) | 1.45 | No. 5 | 67.5 (465) | 102.4 (706) | 1.52 | No. 3 | 125.3 (864) | 152.5 (1051) | 1.22 | 7.42 (51.2) | 7.15 (49.3) |
| | No. 4 | 66.3 (457) | 96.1 (663) | 1.45 | | | | | | | | | | | | | | |
| HHC_0.5H | No. 4 | 122.7 (846) | 150.6 (1038) | 1.23 | No. 4 | 122.7 (846) | 150.6 (1038) | 1.23 | No. 4 | 122.7 (846) | 150.6 (1038) | 1.23 | No. 3 | 125.3 (864) | 152.5 (1051) | 1.22 | 7.30 (50.3) | 7.16 (49.4) |
| HHH_0.5H | No. 4 | 122.7 (846) | 150.6 (1038) | 1.23 | No. 4 | 122.7 (846) | 150.6 (1038) | 1.23 | No. 4 | 122.7 (846) | 150.6 (1038) | 1.23 | No. 3 | 125.3 (864) | 152.5 (1051) | 1.22 | 11.23 (77.4) | 10.69 (73.7) |
| HHH_1.0H | No. 5 | 125.5 (865) | 151.3 (1043) | 1.21 | No. 4 | 125.0 (862) | 151.2 (1042) | 1.21 | — | — | — | — | No. 3 | 127.1 (876) | 155.0 (1069) | 1.22 | 10.80 (74.5) | 10.91 (75.2) |
| CCC_1.5H | No. 11 | 66.2 (456) | 97.9 (675) | 1.48 | No. 4 | 68.6 (473) | 97.5 (672) | 1.42 | — | — | — | — | No. 3 | 70.2 (484) | 99.8 (688) | 1.42 | 7.74 (53.4) | 6.27 (43.2) |
| HCC_1.5H | No. 9 | 101.9 (703) | 134.1 (925) | 1.32 | No. 4 | 125.0 (862) | 151.2 (1042) | 1.21 | — | — | — | — | No. 3 | 70.2 (484) | 99.8 (688) | 1.42 | 7.87 (54.3) | 5.76 (39.7) |
| HHH_1.5H | No. 9 | 101.9 (703) | 134.1 (925) | 1.32 | No. 4 | 125.0 (862) | 151.2 (1042) | 1.21 | — | — | — | — | No. 3 | 127.1 (876) | 155.0 (1069) | 1.22 | 12.77 (88.0) | 14.69 (101) |
| CCC_1.5M | No. 7 | 64.7 (446) | 96.9 (668) | 1.50 | No. 3 | 62.6 (432) | 91.3 (629) | 1.46 | — | — | — | — | No. 3 | 62.6 (432) | 91.3 (629) | 1.46 | 4.43 (30.5) | 4.35 (30.0) |
| HCC_1.5M | No. 5 | 117.0 (807) | 145.6 (1004) | 1.24 | No. 3 | 115.9 (799 | 141.0 (972) | 1.22 | — | — | — | — | No. 3 | 62.6 (432) | 91.3 (629) | 1.46 | 4.77 (32.9) | 4.82 (33.2) |

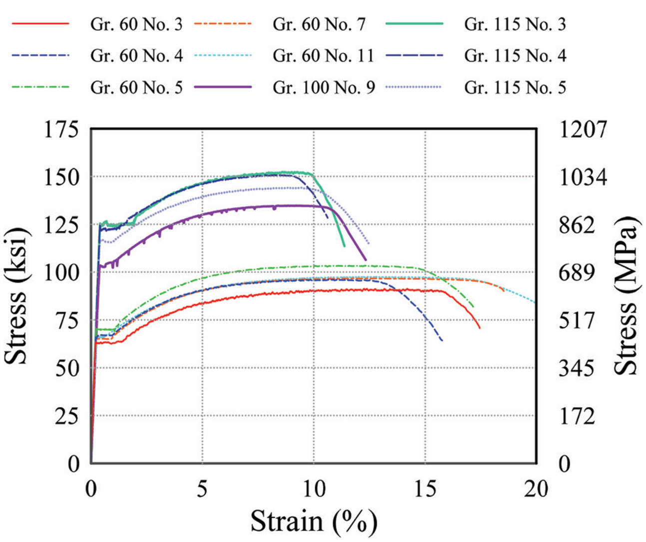


*Fig. 3—Sample stress–strain relationship of reinforcement.*

was insisted so that all specimens had the same confinement reinforcement and was not expected to affect test results.

$$V_{n1} = A_{cv}(3.0\sqrt{f_c'} + \rho_t f_y) \leq 10\sqrt{f_c'}\, A_{cv} \text{ [in psi]} \quad (1a)$$

$$V_{n1} = A_{cv}(0.25\sqrt{f_c'} + \rho_t f_y) \leq 0.83\sqrt{f_c'}\, A_{cv} \text{ [in MPa]} \quad (1b)$$

$$V_{n2} = 0.6 A_{vf} f_y \leq \min\ \{0.2 f_c'\, A_{cv},\ 800 A_{cv}\} \text{ [in psi]} \quad (2a)$$

$$V_{n2} = 0.6 A_{vf} f_y \leq \min\ \{0.2 f_c'\, A_{cv},\ 5.5 A_{cv}\} \text{ [in MPa]} \quad (2b)$$

## Test setup and displacement history

The setup used for the testing of the wall specimens is shown in Fig. 4. This setup allowed lateral displacements to be applied at the top of the specimen with hydraulic actuators, imposing in-plane, single-curvature deformations to the test specimen with negligible axial force. The target lateral displacement history is illustrated in Fig. 5, where drift is defined as the applied lateral displacement divided by the specimen height, $h_w$, measured from the center of the displacement application to the base of the wall.

## Instrumentation

Specimen external deformations were recorded using linear variable differential transformers (LVDTs) and an optical system that tracked the movement of "markers" attached to the specimen surface. The locations of LVDTs and markers are schematically shown in Fig. 6. One LVDT was used to measure the lateral movement of the top concrete block at a level corresponding to the centerline of the hydraulic actuators, while the other LVDT measured lateral movement at the mid-height of the concrete base block. Markers were attached to the specimen in a nominally 12 in. (300 mm) grid pattern. Some markers were attached on the concrete base block to track its lateral movement and rotation. Strains in the steel reinforcement were measured at various locations using 43, 47, and 57 strain gauges for the specimens with $h_w/l_w$ of 0.5, 1.0, and 1.5, respectively.

## TEST RESULTS

### Damage progress

Horizontal and inclined cracks developed in all test specimens during the first cycle to a 0.25% target drift. Horizontal cracks were mainly observed within the boundary elements. Inclined cracks formed as extensions of the horizontal cracks toward the base of the other side of the wall.

For specimens with $h_w/l_w$ of 0.5, noticeable deterioration along the cracks was observed during the 0.75% drift cycles. Slight spalling of concrete cover was observed in the web region, near wall mid-length and at the level corresponding to the termination of the dowel reinforcement, where two inclined cracks intersected. Specimens with USD785 web reinforcement (HHC_0.5H and HHH_0.5H) had fewer but wider cracks compared to specimens with Grade 60 web reinforcement (CCC_0.5H and CHC_0.5H). During 1.00% target drift cycles, spalling of cover concrete progressed horizontally for CCC_0.5H and CHC_0.5H. Horizontal cracks that had formed in both loading directions, near the termination of the dowel reinforcement, joined to form a major horizontal crack across the whole wall length. For HHC_0.5H and HHH_0.5H, during the 1.00% target drift cycles, spalling of concrete progressed both horizontally to the wall edges and diagonally to the upper corners of the wall. In the 1.50% target drift cycles, severe specimen deterioration was observed in specimens with $h_w/l_w$ of 0.5, as shown in Fig. 7(a) to (d). Horizontal failure planes near the level of the dowel reinforcement termination were evident in CCC_0.5H and CHC_0.5H. For HHC_0.5H, damage was more apparent along a few major inclined cracks that

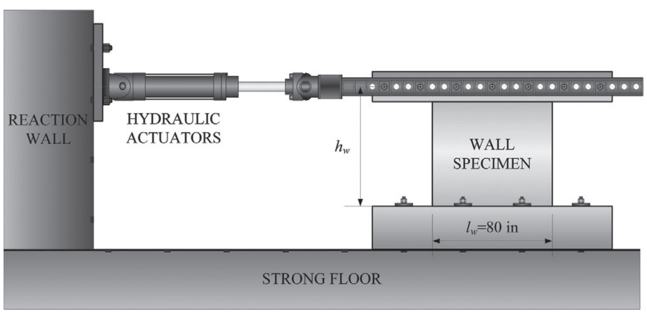


Fig. 4—Test setup.

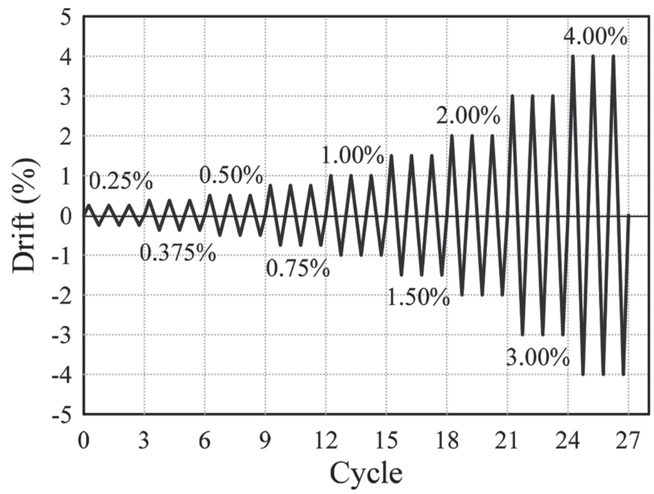


Fig. 5—Loading history.

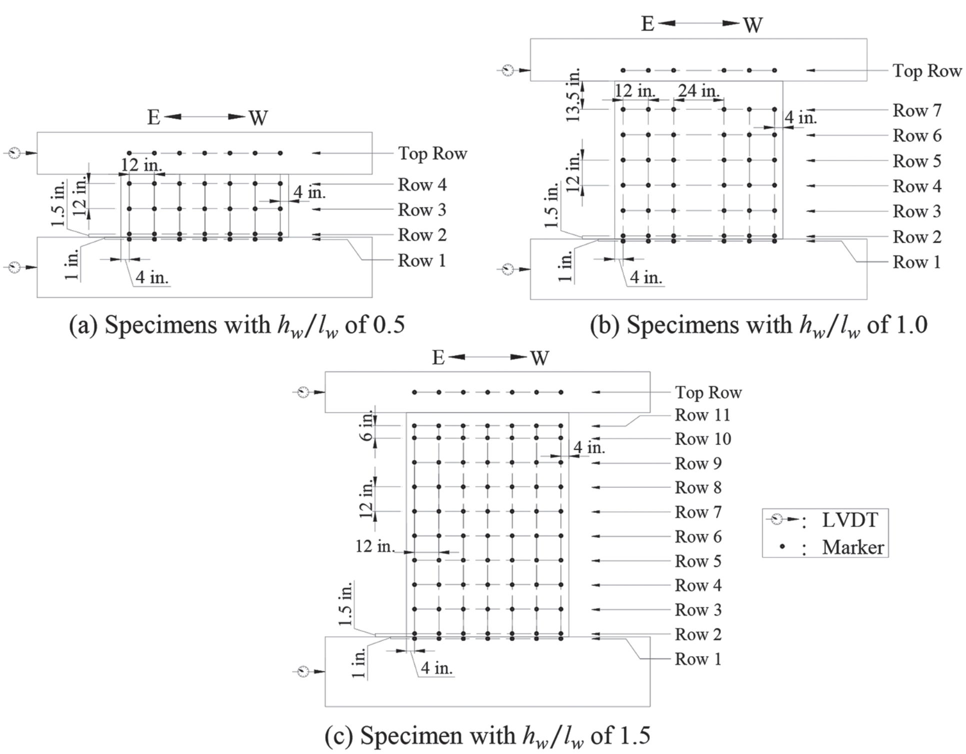


Fig. 6—Instrumentation.

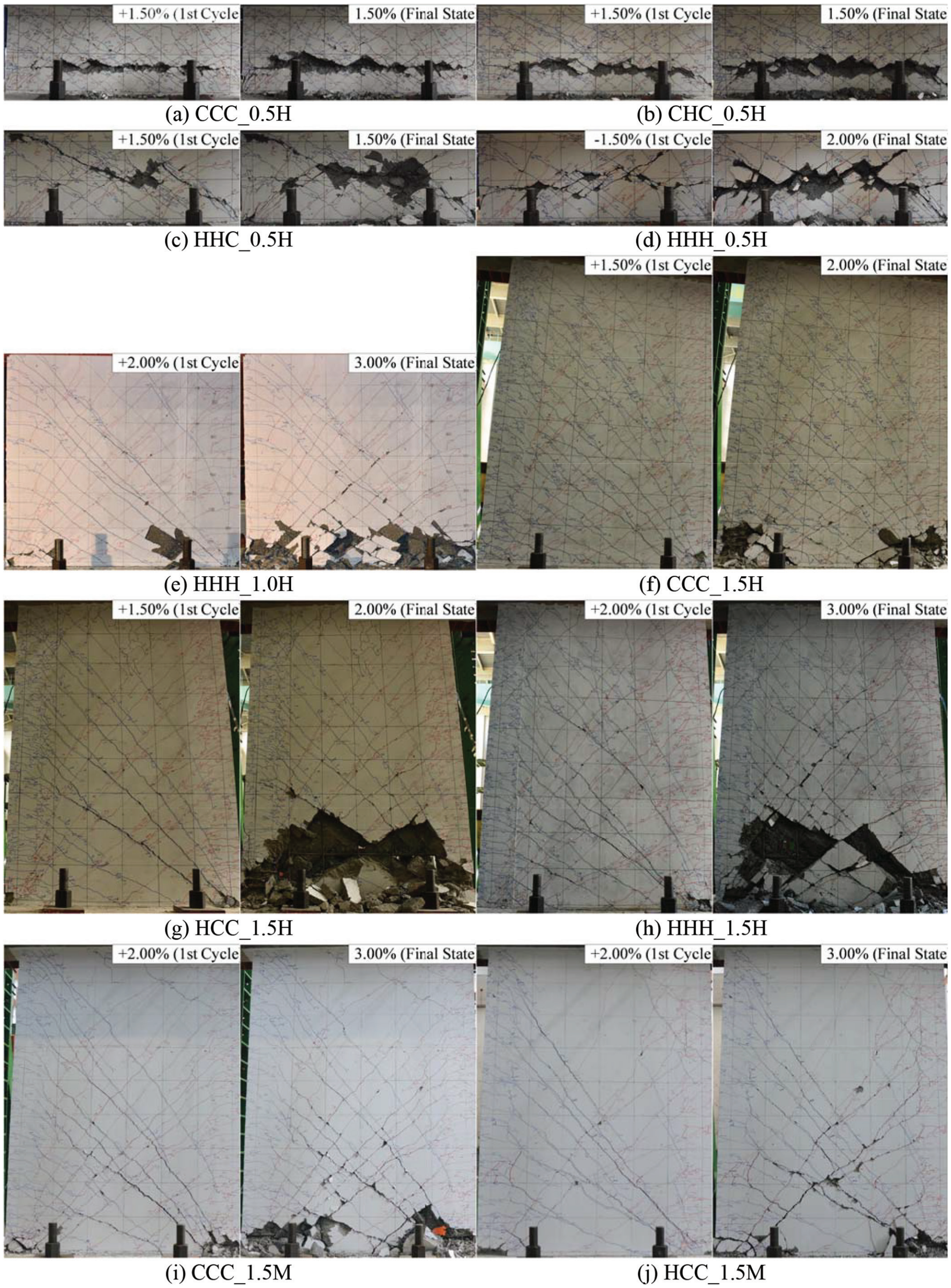


*Fig. 7—Damage states.*

progressed from the wall mid-length, on the level corresponding to the termination of the dowel reinforcement, to the upper corners of the walls. For HHH_0.5H, concrete damage developed along the inclined and horizontal cracks. Relative sliding displacements along these respective cracks became clearly visible during the repeated cycles of 1.50% target drift. After testing, deterioration of concrete near the corners of the walls, within the boundary elements, was observed in every specimen, but with different degrees of damage; (refer to Fig. 7(a) to (d)). Web concrete within the area with dowel reinforcement was relatively intact.

Most horizontal and inclined cracks in HHH_1.0H developed after the completion of cycles to 0.75% target drift. Spalling of concrete cover was first observed at the corner of the wall during the first cycle to 1.50% target drift. During the second cycle to that drift, some spalling of cover concrete was observed in the lower part of the web region, close to the edge of the special boundary elements. Further concrete deterioration was observed in this region and near the base of the boundary elements as the loading progressed, as shown in Fig. 7(e). During the 3.00% target drift cycles, concrete deterioration near the base of the wall worsened, which resulted in apparent sliding near the base, as depicted in Fig. 7(e).

For specimens with an $h_w/l_w$ of 1.5, most cracks developed after the completion of 0.75% target drift cycles. At similar drift demands, the extent of horizontal cracking in the specimens was similar. However, inclined cracks in specimens with moderate shear demands (CCC_1.5M and HCC_1.5M) were only observed up to the mid-height of the specimens, while inclined cracks in specimens with high shear demands (CCC_1.5H, HCC_1.5H, HHH_1.5H) occurred along the full specimen height. New horizontal and inclined cracks were observed as the loading progressed. During the third cycle of 1.00% target drift, cover concrete at the corner of the wall base exhibited distress in CCC_1.5H, HCC_1.5H, and CCC_1.5M. At this drift level, concrete distress was not apparent in HHH_1.5H and HCC_1.5M. During the 1.50% target drift cycles, severe concrete deterioration at the corners of CCC_1.5H and HCC_1.5H was observed, but the damage to HCC_1.5H was more severe. For CCC_1.5H, sliding was very apparent in the second and third cycles to 1.50% target drift. In HCC_1.5H, a few inclined cracks became much wider. Due to this concentration of damage, as depicted in Fig. 7(g), a triangular piece of relatively undamaged concrete that appeared to limit sliding deformations in HCC_1.5H was left near the wall base. For HHH_1.5H and HCC_1.5M, only slight spalling of cover concrete was observed at the wall corners at the end of the 1.50% target drift cycles. Concrete deterioration at the corners of CCC_1.5M was also observed during the 1.50% target drift cycles and was relatively more severe compared to HHH_1.5H and HCC_1.5M.

Testing of CCC_1.5H and HCC_1.5H was terminated after completion of the first 2% target drift cycles due to significant loss of lateral force. The final states of the two specimens are shown in Fig. 7(f) and (g). Damage patterns in HHH_1.5H, CCC_1.5M, and HCC_1.5M were similar during the 2.00% target drift cycles, where inclined crack widths increased, and concrete deteriorated further at wall corners. However, the extent of damage in HHH_1.5H was the worst among the three after the 2.00% target drift cycles.

In the 3.00% target drift cycles, further concrete deterioration at the wall corners and crack widening were observed in HHH_1.5H, CCC_1.5M, and HCC_1.5M. However, HHH_1.5H exhibited the worst concrete deterioration among the three, in which severe deterioration of concrete was mainly concentrated along the main inclined cracks that extended from the corners of the wall base to the point where the main inclined cracks in both loading directions intersected, leaving a relatively intact central triangular section near the base. The test was terminated after completion of the first cycle in HHH_1.5H. For CCC_1.5M, however, concrete deterioration at the wall base extended inward from the boundary elements to the middle of the web during the 3.00% target drift cycles. The loss of core concrete in both the boundary elements and web section created a weak plane near the wall base, where significant sliding was observed. For HCC_1.5M, concrete continued to deteriorate, but the damage was more concentrated at the corners of the wall base, which caused the loss of core concrete in the boundary elements. Concrete within the web section of HCC_1.5M was still relatively intact but sliding along the base was apparent in the later drift cycles. Tests were terminated at the end of the 3.00% target drift cycles for both CCC_1.5M and HCC_1.5M. The final states of specimens with $h_w/l_w$ of 1.5 are presented in Fig. 7(f) to (j).

## Hysteresis

The normalized shear stress versus drift hysteresis responses of all specimens is presented in Fig. 8. Unless noted, the drifts in Fig. 8 and later in this article are adjusted to account for lateral movement and rotation of the concrete base block, except for HHH_0.5H where the optical tracking system malfunctioned during the test. The difference between the target and the adjusted drift was typically within 5% of the target drift. To illustrate this difference, adjusted and target values in CCC_0.5H are presented in Fig. 8(a).

Key test results are summarized in Table 4. For comparison, test results of four specimens (M60, H60, M115, and H115) from Cheng et al.[3] are included in Table 4. In Table 4, $V_p$, $d_p$, and $d_u$ are the average values of the peak lateral loads, drift ratios at peak loads, and drift capacities, respectively, in both positive and negative loading directions. Drift capacity in each loading direction was determined as the lesser of the drift at which 1) an envelope connecting the peaks of the first cycle to each target drift had a lateral load that was less than 80% of the peak load or 2) repeated cycles had strengths less than 80% of the peak load of the first cycle and the first cycle peak load of the next target drift cycle was lower than the peak load of the third cycle of the drift level in question.

*Strength*—The average of the peak lateral loads, $V_p$, in the positive and negative loading directions for each specimen is listed in column 2 of Table 4. As can be seen in column 7, for specimens with $h_w/l_w$ of 1.0 and 1.5, $V_p$ was close to $V_{mn}$, the shear associated with the development of nominal flexural strength at the wall base, with mean and coefficient of variation values for $V_p/V_{mn}$ of 1.04 and 0.045, respectively. For these specimens, $V_p$ was approximately 10% less than $V_{mpr}$, as presented in column 8, with mean and coefficient of variation values for $V_p/V_{mpr}$ of 0.91 and 0.028, respectively.

For specimens with $h_w/l_w$ of 0.5, $V_{mn}$ and $V_{mpr}$ were evaluated at two sections: 1) where dowel reinforcement was terminated (dowel end) and 2) at the base of the wall. As shown in Table 4, regardless of the material strengths, none of the specimens with $h_w/l_w$ of 0.5 achieved $V_{mn}$ at either section. However, strain gauge readings in most of those specimens indicated that vertical reinforcement in the special boundary elements exceeded the yield strain at a few locations after completion of the 0.50% target drift cycles—before the specimens achieved the peak lateral strength. The shear associated with the yield flexural strength, $V_{my}$, was therefore also considered and results are presented in column 6 of Table 4. The yield flexural strength was estimated as the moment when the outermost layer of vertical tensile reinforcement achieved first yielding, where yielding strain was determined using the measured $f_y$ divided by the steel elastic modulus of 29,000 ksi (200,000 MPa). Yield flexural strength was determined using the Hognestad[8] concrete model and the elastic-perfectly plastic steel model. Specimens yielding flexural strength is not sensitive to the material model selected. As shown in column 6 of Table 4, the peak strengths, $V_p$, of specimens with an $h_w/l_w$ of 0.5 were close to $V_{my}$ at the wall base. For these specimens, $V_p$ was less than the nominal shear strengths calculated using the ACI 318-14, $V_{n1}$ and $V_{n2}$, as shown in columns 9 and 10.

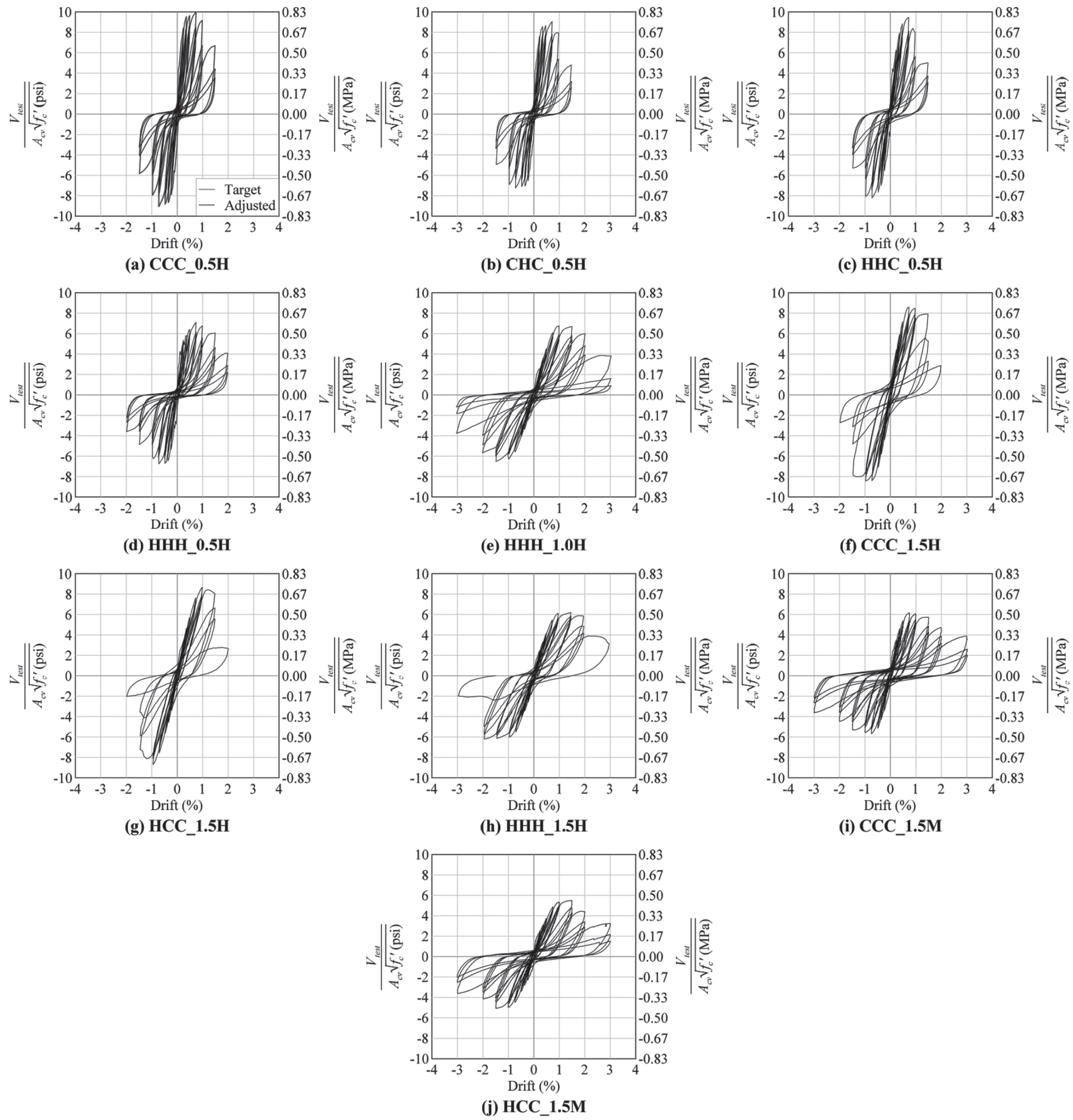


*Fig. 8—Hysteretic responses.*

Overall, specimens with high-strength reinforcement (either USD685 or USD785) exhibited strengths like specimens with conventional Grade 60 reinforcement, provided that the total steel force (total steel area times the steel yield strength) was similar. Increasing concrete strength slightly increased $V_p$ in specimens with $h_w/l_w$ of 1.0 and 1.5. However, peak strengths of specimens HHC_0.5H and HHH_0.5H were not positively correlated with the concrete strength. This indicates that peak strength of specimens with $h_w/l_w$ of 0.5 was likely to be more associated with the steel strength than concrete strength.

*Deformation*—The relationship between normalized shear demand and average ultimate drift capacity, $d_u$, for all specimens tested in this study is presented in Fig. 9, together with four specimens from Cheng et al.[3] As depicted in Fig. 9, the general trend agrees with the findings of previous studies[3,9] and clearly shows that specimen drift capacity increases as the normalized shear demand decreases.

Specimens with high-strength reinforcement (either USD685 or USD785) exhibited deformation capacities similar to the corresponding specimens with conventional Grade 60 reinforcement when steel force was similar. Increasing concrete strength reduced the normalized shear stress demand, which was correlated with improved specimen deformation capacity. Results from CCC_0.5H and CHC_0.5H show that increasing confinement steel strength while maintaining other design parameters appears to have a negligible effect on the deformation capacity.

The deformation components of the wall section (sliding at the base, strain penetration, shear, and flexure) were determined using data from the optical tracking system. Results are shown in Fig. 10 in terms of percentage of total drift at the peak of the first cycle of every target drift. Strain penetration and sliding, defined as the deformation due to rotation and slip at base of the wall, respectively, were calculated using markers above and below the interface between the wall and base concrete block, that is, Rows 1 and 2 markers

### Table 4–Summary of test results

| Specimen name | | $V_p$, kip (kN) | $V_p/A_{cv}\sqrt{f_{cm}'}$, psi (MPa) | $d_p$, % | $d_u$, % | $V_p/V_{my}$ | $V_p/V_{mn}$ | $V_p/V_{mpr}$ | $V_p/V_{n1}$ | $V_p/V_{n2}$ |
|---|---|---|---|---|---|---|---|---|---|---|
| (1) | | (2) | (3) | (4) | (5) | (6) | (7) | (8) | (9) | (10) |
| CCC_0.5H | Dowel end | 431.3 (1919) | 9.53 (0.79) | 0.73 | 1.18 | 1.23 | 0.84 | 0.75 | 0.95 | 0.77 |
| | base | | | | | 1.03 | 0.66 | 0.60 | | 0.87 |
| CHC_0.5H | Dowel end | 427.6 (1902) | 8.16 (0.68) | 0.72 | 1.17 | 1.19 | 0.81 | 0.73 | 0.85 | 0.71 |
| | base | | | | | 0.98 | 0.62 | 0.57 | | 0.86 |
| HHC_0.5H | Dowel end | 463.1 (2060) | 8.83 (0.74) | 0.72 | 1.01 | 1.09 | 0.79 | 0.71 | 0.97 | 0.75 |
| | base | | | | | 1.04 | 0.71 | 0.66 | | 0.93 |
| HHH_0.5H | Dowel end | 444.0 (1975) | 6.93 (0.58) | 0.72 | 1.41 | 1.03 | 0.73 | 0.66 | 0.86 | 0.72 |
| | base | | | | | 0.96 | 0.63 | 0.58 | | 0.90 |
| HHH_1.0H | | 429.7 (1911) | 6.64 (0.55) | 1.24 | 2.02 | 1.24 | 1.02 | 0.94 | 0.82 | 0.87 |
| M60[3] | | 247.0 (1099) | 5.28 (0.44) | 0.66 | 2.68 | 1.22 | 1.08 | 0.95 | 0.92 | 0.80 |
| M115[3] | | 241.0 (1072) | 5.24 (0.44) | 1.17 | 3.21 | 1.32 | 1.11 | 0.92 | 0.97 | 0.82 |
| H60[3] | | 408.5 (1817) | 8.24 (0.69) | 0.73 | 1.62 | 1.29 | 1.00 | 0.89 | 0.82 | 0.82 |
| H115[3] | | 396.5 (1764) | 7.99 (0.67) | 1.35 | 1.90 | 1.34 | 1.09 | 0.92 | 0.87 | 0.80 |
| CCC_1.5H | | 417.6 (1857) | 8.51 (0.71) | 0.85 | 1.58 | 1.19 | 0.98 | 0.88 | 0.85 | 0.84 |
| HCC_1.5H | | 408.1 (1815) | 8.67 (0.72) | 0.97 | 1.47 | 1.18 | 0.99 | 0.87 | 0.87 | 0.82 |
| HHH_1.5H | | 465.3 (2070) | 6.19 (0.52) | 1.70 | 2.27 | 1.29 | 1.07 | 0.93 | 0.84 | 0.94 |
| CCC_1.5M | | 241.9 (1076) | 5.92 (0.49) | 0.75 | 1.90 | 1.27 | 1.06 | 0.92 | 0.99 | 0.52 |
| HCC_1.5M | | 227.5 (1012) | 5.29 (0.44) | 1.49 | 2.04 | 1.24 | 1.07 | 0.92 | 0.95 | 0.52 |

Note: $V_{my}$ is shear demand associated with the development of yield flexural capacity, determined using material test results with Hognestad[8] concrete model and elastic-perfectly plastic steel model for steel reinforcement; $V_{mn}$ is shear demand associated with the development of nominal flexural capacity, determined using material test results with equivalent rectangular stress block for concrete and elastic-perfectly plastic steel model for steel reinforcement; $V_{mpr}$ is shear demand associated with the development of the probable flexural capacity, determined using concrete cylinder strength and 1.25 times the specified yield strength for Grade 60 steel and 1.20 times the specified yield strength for USD685 and USD785 steels; and $V_{n1}$ and $V_{n2}$ are determined on basis of tested material strengths.

in Fig. 6. Flexural deformation was evaluated using markers between Row 2 and the topmost row of markers on the wall (for example, Row 4 in Fig. 6(a)). Shear deformation refers to the rest of the deformation between Row 2 and the topmost row of markers on the wall.

As indicated by Cheng et al.,[3] the contribution of sliding deformation at the wall base was highly correlated with the extent of yielding of the flexural reinforcement. This is shown by the results from specimens with $h_w/l_w$ of 1.5, where specimens with high-strength flexural reinforcement typically exhibited smaller sliding deformations than the companion specimens with conventional reinforcement at similar drift demands (compare HCC_1.5H with CCC_1.5H and HCC_1.5M with CCC_1.5M). When reinforcement grade was identical, sliding deformations tended to be larger for specimens with less shear stress demand. This may be because yielding was more extensive in specimens with less flexural reinforcement or because specimens with high shear

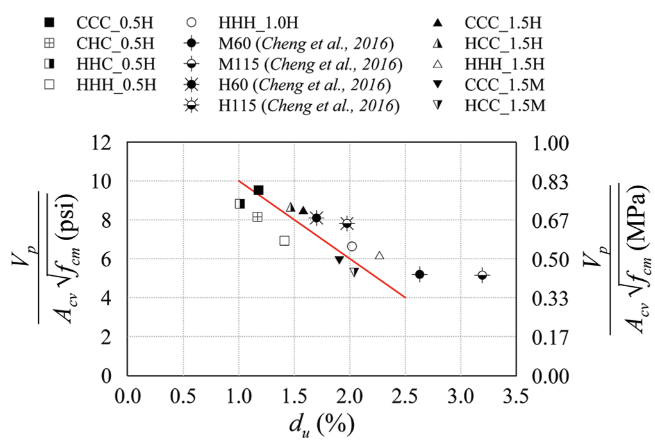


*Fig. 9—Normalized shear demand versus average ultimate drift capacity.*

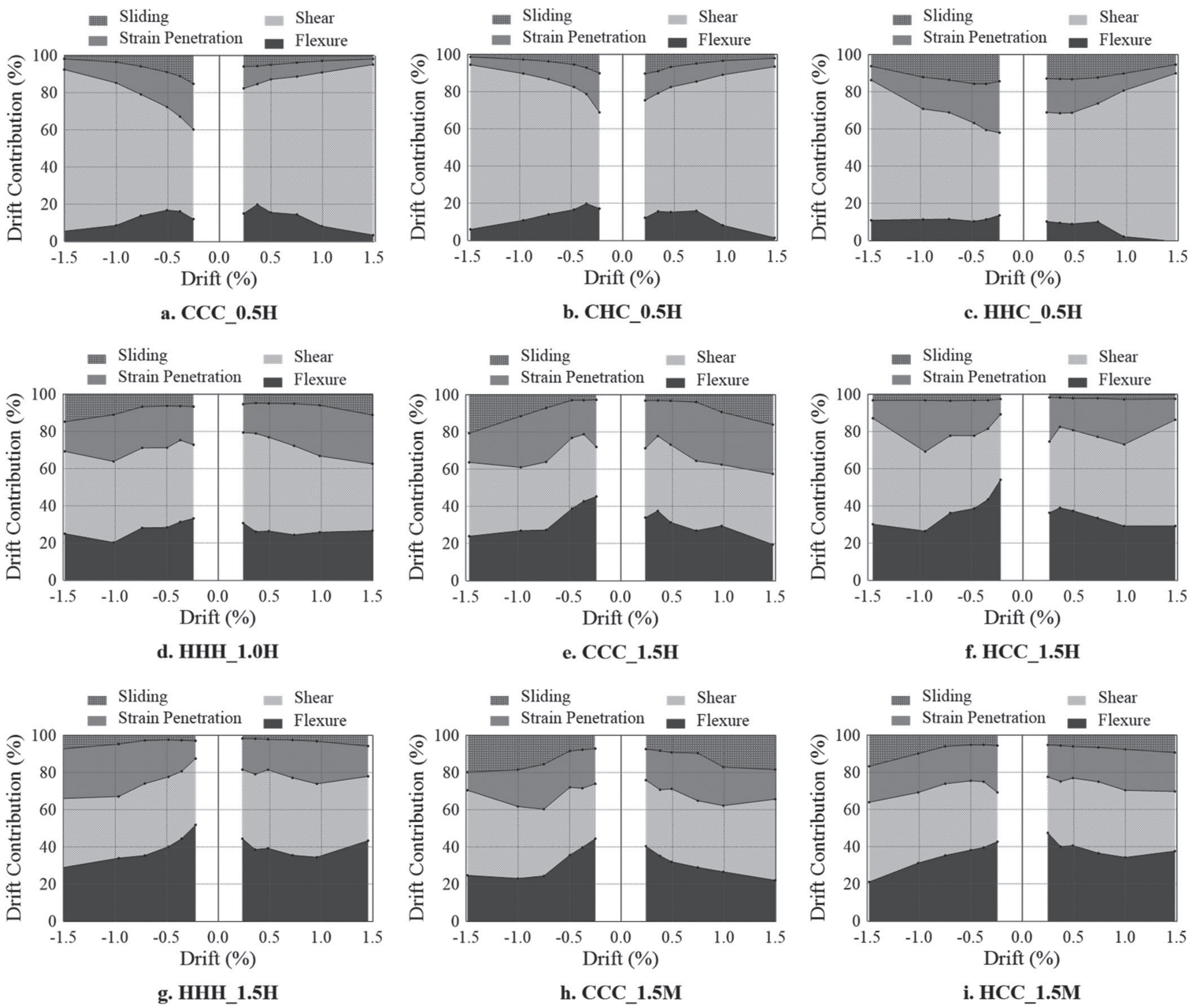


*Fig. 10—Deformation components.*

stresses had more widely distributed cracking and damage. However, results from specimens with $h_w/l_w$ of 0.5 did not follow the trend, perhaps because sliding deformations concentrated away from the base, which was reinforced with dowel reinforcement.

Deformation due to strain penetration includes the effects of slip and extension of tensile flexural reinforcement in the anchorage zone (base block). The use of high-strength bars, which requires longer development lengths, likely results in larger contributions from strain penetration to overall drift. Figure 11 shows the bond stress demand for each specimen versus wall base rotation due to strain penetration and slip calculated when the specimens approximately reached their yield flexural strength. In Fig. 11, the bond stress demand is expressed as $A_b f_y/\pi d_b\sqrt{f_{cm}}$ , where $A_b$ is the bar nominal area, $f_y$ is the tested steel yield stress, $d_b$ is the bar nominal diameter, and $f_{cm}$ is the tested compressive strength for the base block concrete. If a uniform bond stress (of magnitude $x\sqrt{f_{cm}}$) is assumed to act on the surface of the bars within the base block, then bar stress will vary from $f_y$ at the base of the wall to zero at some distance $\ell$ into the block. For this scenario, the ratio presented in the vertical axis of Fig. 11 corresponds to $x\ell$. Higher strength bars have a larger $A_b f_y$ and thus require a larger value of $x\ell$ (effectively, a longer development length). Figure 11 shows clearly that larger $x\ell$ is correlated with $\theta_{sp}$.

Figure 10 also shows that the contributions of shear and flexural deformations to drift were similar regardless of steel grade or shear stress demand among specimens with the same $h_w/l_w$. However, the relative importance of shear and flexural deformations was highly correlated to $h_w/l_w$. For specimens with $h_w/l_w$ of 1.5, the contributions of flexural and shear deformations before the specimens achieved peak strength accounted for about 35% and 25% of the overall deformation, respectively, regardless of the steel grade and shear stress demand. As $h_w/l_w$ decreased, shear deformations became increasingly significant, with approximately 70% of drift in specimens with $h_w/l_w$ of 0.5 attributable to shear deformation near peak strength.

*Flexural and shear stiffnesses*—Using the calculated flexural and shear deformations reported in the previous section, the effective flexural and shear stiffnesses can be evaluated. The experimental flexural stiffness, $EI_f$, was calculated using Eq. (3), while the experimental shear stiffness, $GA_s$, was calculated using Eq. (4). Both $EI_f$ and $GA_s$ were determined using the deformations calculated when the ascending branch of the shear-drift envelope reached 60% of the peak load in the positive direction. The corresponding values of $EI_f/E_cI_g$ and $GA_s/G_cA_{cv}$ in the positive loading direction are

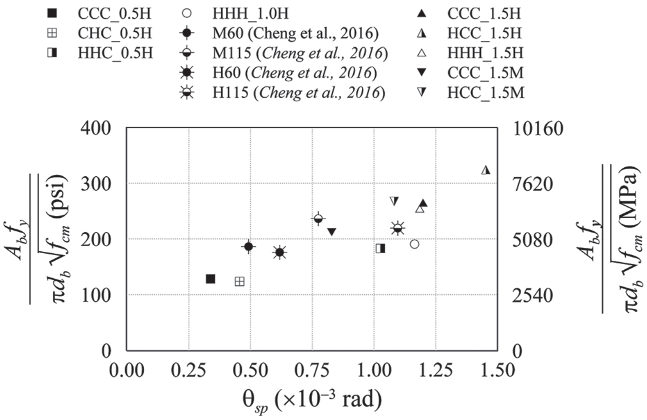


*Fig. 11—Bond demand versus wall-base rotation due to strain penetration.*

presented in Fig. 12 and 13, respectively, where $E_c$ is taken as $57,000\sqrt{f_{cm}}$ (psi) or $4700\sqrt{f_{cm}}$ (MPa), $I_g$ is the moment of inertia of the gross section neglecting reinforcement, $G_c$ is estimated as $0.43E_c$, and $A_{cv}$ is the wall cross-sectional area.

$$EI_f = (L^2/12\Delta_f) \times [V_{60}L + 3(M_{top} + M_2)] \quad (3)$$

$$GA_s = V_{60}/\Delta_s L \quad (4)$$

Figure 12 indicates that 1) flexural stiffness appears to increase as $h_w/l_w$ increases, 2) the cracked stiffness of $0.35E_cI_g$ suggested in ACI 318-14 overestimates the flexural stiffness for specimens with $h_w/l_w$ of 0.5 but underestimates the flexural stiffness for specimens with $h_w/l_w$ of 1.5, and 3) specimens with high-strength steel typically had smaller $EI_f/E_cI_g$ than specimens with Grade 60 steel when the specimens were designed to have equivalent steel force and the same $h_w/l_w$.

Figure 13 indicates that 1) shear stiffness is greater for $h_w/l_w = 0.5$ than for $h_w/l_w = 1.5$; 2) $1.0G_cA_{cv}$ suggested in ACI 318-14, which neglects the effects of cracking, dramatically overestimates shear stiffness, and 3) specimens with high-strength steel typically have smaller $GA_s/G_cA_{cv}$ than specimens with Grade 60 steel when the specimens are designed to have equivalent steel force.

The flexural stiffness of $0.35E_cI_g$ and shear stiffness based on the whole section area for structural analysis were first included in ACI 318 in 1995.[10] These two values remain, unchanged, in ACI 318-14. Test results from this study showed the two suggested values may have room for improvement.

## CONCLUSIONS

This study extends the experimental work reported by Cheng et al.[3] by reporting results from tests of 10 additional RC squat wall specimens constructed with conventional and high-strength reinforcement and concrete. Variables included $h_w/l_w$, steel grade, concrete compressive strength, and shear stress demand. The following conclusions are drawn:

1. For $0.5 \leq h_w/l_w \leq 1.5$, specimens with high-strength reinforcement exhibited strength and deformation capacities similar to specimens with conventional Grade 60 reinforcement when the specimens were designed to have equivalent steel force (total steel area times the steel yield stress).

2. The peak strength of specimens with $h_w/l_w$ of 1.0 or 1.5 can be estimated as the shear associated with the nominal flexural strength at the wall base, $V_{mn}$, when the nominal shear strength exceeds $V_{mn}$. The peak strength of specimens with $h_w/l_w$ of 0.5 is best estimated as the shear associated with the yield flexural strength at the wall base when the nominal shear strength exceeds $V_{mn}$.

3. Deformation capacity increases as the normalized shear stress decreases. The use of high-strength concrete leads to lower normalized shear stress demand and, therefore, larger deformation capacity.

4. Flexural stiffness appears to increase as $h_w/l_w$ increases. The cracked flexural stiffness of $0.35E_cI_g$ suggested in ACI 318-14 overestimates the flexural stiffness for specimens with $h_w/l_w$ of 0.5 but underestimates the flexural stiffness for specimens with $h_w/l_w$ of 1.5. Shear stiffness of test specimen

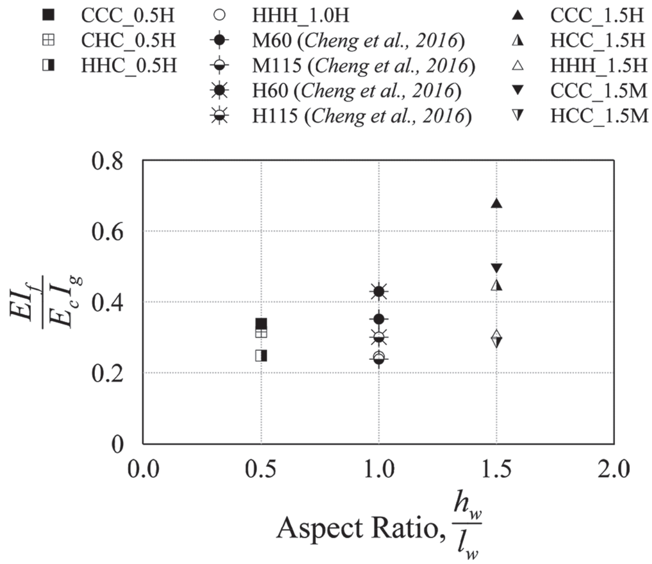


*Fig. 12—Flexural stiffness versus aspect ratio.*

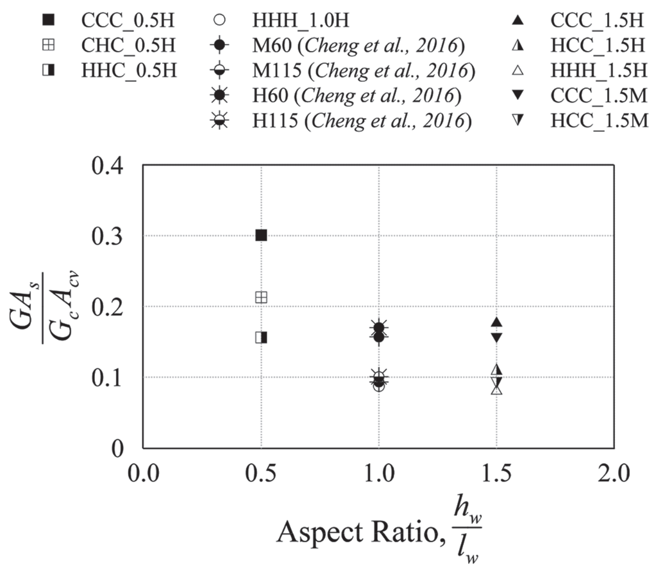


*Fig. 13—Shear stiffness versus aspect ratio.*

ranges approximately from $0.1G_cA_{cv}$ to $0.3\ G_cA_{cv}$, which is significantly lower than the $1.0G_cA_{cv}$ suggested in ACI 318-14.

## AUTHOR BIOS

*ACI member* **Min-Yuan Cheng** *is Professor of Civil and Construction Engineering at National Taiwan University of Science and Technology, Taipei, Taiwan. He is a member of ACI Subcommittees 318-J, Joints and Connections, and 318-L, International Liaison; and Joint ACI-ASCE Committee 352, Joints and Connections in Monolithic Concrete Structures.*

**Leonardus S. B. Wibowo** *is Lecturer in Civil Engineering Department at Widya Kartika University in Surabaya, Indonesia. He received his BS in civil engineering from Brawijaya University, Malang, Indonesia, MS in civil engineering from Sepuluh Nopember Institute of Technology, Surabaya, Indonesia, and PhD in civil and construction engineering at National Taiwan University of Science and Technology, Taipei, Taiwan.*

*ACI member* **Marnie B. Giduquio** *is Project Assistant Professor in the Department of Civil and Construction Engineering at National Taiwan University of Science and Technology, Taipei, Taiwan. He received his BS degree in civil engineering from University of San Carlos, Cebu City, Philippines and his MS and PhD in civil and construction engineering from National Taiwan University of Science and Technology, Taipei, Taiwan.*

*ACI member* **Rémy D. Lequesne** *is Associate Professor of Civil, Environmental, and Architectural Engineering at the University of Kansas, Lawrence, KS. He is Chair of Joint ACI-ASCE Committee 408, Bond and Development of Steel Reinforcement, and a member of ACI Subcommittee 318-J, Joints and Connections, and Joint ACI-ASCE Committee 352, Joints and Connections in Monolithic Concrete Structures.*

## ACKNOWLEDGMENTS

The authors thank the Japanese steel manufacturer Tokyo Tekko Co. for the support in this research project and for supplying the reinforcing steel. All tests were conducted at the National Center for Research on Earthquake Engineering (NCREE). The authors express their gratitude to the staff at NCREE for their help.

## NOTATION

$A_{cv}$ = gross area of concrete bounded by $l_w$ and $b_w$
$A_{vf}$ = total area of vertical reinforcement crossing horizontal shear plane
$b_w$ = width (thickness) of wall
$d_p$ = average of drift ratios at peak strength in positive and negative loading directions
$d_u$ = average of drift capacities in positive and negative loading directions
$E/I_f$ = effective flexural stiffness
$E_c$ = concrete modulus of elasticity equivalent to $57{,}000\sqrt{f_{cm}}$(psi) or $4700\sqrt{f_{cm}}$(MPa)
$f_c'$ = specified concrete compressive strength
$f_{cm}$ = measured average concrete compressive strength
$f_p$ = peak stress of reinforcement
$f_y$ = yield stress of reinforcement
$GA_s$ = effective shear stiffness
$G_c$ = concrete shear modulus taken as $E_c/2(1+0.15) = 0.43E_c$
$h_w$ = height of wall, measured from center of actuator force to top face of concrete base block
$I_g$ = moment of inertia of gross concrete section about centroidal axis, neglecting reinforcement
$L$ = vertical height between second and topmost row of markers on wall
$\ell$ = nominal development length within concrete base block when uniform bond stress is assumed
$l_w$ = length of wall
$M_n$ = nominal flexural strength, determined using elastic-perfectly plastic steel properties and equivalent concrete compressive stress block
$M_{pr}$ = probable flexural strength, determined using elastic-perfectly plastic steel properties and equivalent concrete compressive stress block, where 1.25 and 1.20 times the yield strength were assumed for Grade 60 and high-strength steel (USD685/USD785), respectively
$M_{top}$ = moment at topmost markers on wall due to $V_{60}$
$M_2$ = moment at second row of markers on wall due to $V_{60}$
$V_{60}$ = 60% of the maximum lateral load in loading direction considered
$V_{mn}$ = shear force associated with development of nominal flexural strength at wall base or at tip of dowel reinforcement (dowel end)
$V_{mpr}$ = shear force associated with development of probable flexural strength at wall base or at tip of dowel reinforcement (dowel end)
$V_{my}$ = shear force associated with development of yield flexural moment at wall base or at tip of dowel reinforcement (dowel end). Yield flexural moment was determined using elastic-perfectly plastic steel properties and the Hognestad[8] concrete model
$V_{n1}$ = nominal web shear strength per ACI 318-14
$V_{n2}$ = nominal shear-friction strength per ACI 318-14
$V_P$ = average of positive and negative peak lateral loads
$x$ = coefficient to present bond stress magnitude in terms of $f_{cm}$
$\Delta_f$ = flexural deformation corresponding to $V_{60}$ in positive loading direction
$\Delta_s$ = shear deformation corresponding to $V_{60}$ in positive loading direction
$\theta_{sp}$ = wall base rotation due to strain penetration/slip at approximately yield flexural moment
$\rho_t$ = horizontal web reinforcement ratio

## REFERENCES

1. ACI Committee 318, "Building Code Requirements for Structural Concrete and Commentary (ACI 318-14)," American Concrete Institute, Farmington Hills, MI, 2014, 519 pp.

2. Park, H. G.; Baek, J. W.; Lee, J. H.; and Shin, H. M., "Cyclic Loading Tests for Shear Strength of Low-Rise RC Walls with Grade 550 MPa Bars," *ACI Structural Journal*, V. 112, No. 3, May-June 2015, pp. 299-310. doi: 10.14359/51687406

3. Cheng, M. Y.; Hung, S. C.; Lequesne, R. D.; and Lepage, A., "Earthquake-Resistant Squat Walls Reinforced with High-Strength Steel," *ACI Structural Journal*, V. 113, No. 5, Sept.-Oct. 2016, pp. 1065-1076. doi: 10.14359/51688825

4. Baek, J. W.; Park, H. G.; Lee, J. H.; and Bang, C. J., "Cyclic Loading Test for Walls of Aspect Ratio 1.0 and 0.5 with Grade 550 MPa (80 ksi) Shear Reinforcing Bars," *ACI Structural Journal*, V. 114, No. 4, July-Aug. 2017, pp. 969-982. doi: 10.14359/51689680

5. ASTM A706/A706M-16, "Standard Specification for Deformed and Plain Low-Alloy Steel Bars for Concrete Reinforcement," ASTM International, West Conshohocken, PA, 2016, 7 pp.

6. Aoyama, H., "Design of Modern Highrise Reinforced Concrete Structures," *Series of Innovation in Structures and Construction*, V. 3, Imperial College, London, 2001, 442 pp.

7. Wibowo, L. S. B.; Cheng, M.-Y.; Huang, F. C.; and Tai, T. Y., "Effectiveness of High-Strength Hoops in High-Strength Flexural Members," *ACI Structural Journal*, V. 114, No. 4, July-Aug. 2017, pp. 887-897. doi: 10.14359/51689620

8. Hognestad, E., "A Study of Combined Bending and Axial Load in Reinforced Concrete Members," *Bulletin Series No. 399*, University of Illinois Engineering Experimental Station, Urbana, IL, Nov. 1951, 128 pp.

9. Athanasopoulou, A., and Parra-Montesinos, G. J., "Experimental Study on the Seismic Behavior of High-Performance Fiber-Reinforced Concrete Low-Rise Walls," *ACI Structural Journal*, V. 110, No. 5, Sept.-Oct. 2013, pp. 767-778.

10. ACI Committee 318, "Building Code Requirements for Structural Concrete and Commentary (ACI 318-95)," American Concrete Institute, Farmington Hills, MI, 1995, 369 pp.